Molecular Catalysis 510 (2021) 111692

Contents lists available at ScienceDirect

Molecular Catalysis

journal homepage: www.journals.elsevier.com/molecular-catalysis

Towards mild conditions by predictive catalysis *via* sterics in the Ru-catalyzed hydrogenation of thioesters

Michele Tomasini [a], Josep Duran [a], Sílvia Simon [a], Luis Miguel Azofra [b,*], Albert Poater [a,*]

[a] Institut de Química Computacional i Catàlisi and Departament de Química, Universitat de Girona, c/ Maria Aurèlia Capmany 69, 17003 Girona, Catalonia, Spain
[b] Instituto de Estudios Ambientales y Recursos Naturales (i-UNAT), Universidad de Las Palmas de Gran Canaria (ULPGC), Campus de Tafira, 35017 Las Palmas de Gran Canaria, Spain

ARTICLE INFO

Keywords:
Homogeneous catalysis
Ruthenium catalysis
Thioesters
Reaction mechanisms
Density functional theory (DFT)

ABSTRACT

The Milstein's reported discovery of hydrogenation of thioesters directly toward thiols and alcohols catalyzed by a Ru-acridine complex has been studied here by DFT calculations to know the origin of the different performance depending on the nature of the substituents. Unveiling the reaction mechanism leads to a deeper understanding of the steric and electronic properties on the nature of the limiting step of the reaction. Steric maps and Conceptual DFT have been the tools to rationalize the reactivity patterns. In addition, the nature of the catalyst has been studied, replacing the substituents on the phosphorous atoms by less sterically demanding groups with the aim to move to milder reaction conditions.

Introduction

In the field of the industrial chemistry, moving from stoichiometric to catalytic reactions represents a primary objective not always achievable. The hydrogenation of thioesters often lies in the stoichiometric consumption of the hydride reagents [1,2], reducing them into thiols and alcohols but also generating waste and presenting low selectivity when thioesters are part of organic substrates with a higher molecular complexity. Undoubtedly, this represents a bottleneck in the applicability of this reaction on biological substrates. In Nature, the four-electrons reduction of thioesters by NAD(P)H in the terminal steps of non-ribosomal peptide synthetase and polyketide synthase allows the biosynthesis of specific alcohols [3–5] from bio-based feedstocks.

Within the sustainable green homogeneous catalytic chemistry, the old methods using stoichiometric amounts of hydride reagents have been replaced by metal-catalyzed reactions for a wide range of substrate transformations [6–10]. While the hydrogenative reactions may lead to the reduction of the organic substrates [11–14], in particular carbamates [15–18], amides [19–21], and any carboxylic derivative group [22–25], here the focus will be on thioesters and the incapacity to hydrogenate them in the past.

In 2020, Milstein and collaborators reported a complex based on ruthenium acridine (**Ru-1**), capable of reducing thioesters, thiocarbamates, and thioamides [26]. As shown at Fig. 1**a**, using hexanethiol, **Ru-1** is transformed into a hydride-thiol Ru based complex (**Ru-2**). In addition (Fig. 1**b**), in presence of a thioester substrate, **Ru-1** generates the corresponding aldehyde and another ruthenium complex, **Ru-3**. As shown at Fig. 1**c**, **Ru-3** has the ability to heterolytically break H_2 under mild conditions, and by reaction with the thioester substrate, the corresponding alcohol and thiol products are generated. Then all efforts were made to convert the already important stoichiometric outputs to catalytic ones. From **Ru-1**, even increasing the pressure of H_2 up to 40 atm, it was not possible to consume the thioester reagent, but the increase in temperature up to 408.15 K allowed to reach up to a full conversion, with yields of 94% of the alcohol and of 96% thiol, completely omitting side reactions. Increasing up to 423.15 K and 10 bar (H_2) the temperature and pressure, respectively, those yields increase up to 95 and 99% (Fig. 1**d**). Furthermore, the substitution of the quasi linear CH_2CH_2Ph of substrate **1a** by the shorter, but at the same time bulkier *t*-butyl group (**1 h**) entailed a drop of 30% of yield (Fig. 1**e**). In addition, it was demonstrated experimentally how hydrogen gas pressure governs selectivity toward hydrogenation or dehydrogenation, together with mechanistic insights [27]. Accordingly, a competing dehydrogenative mechanism was discussed [28–30]. The thermodynamical preference was not enough because of the prohibitive kinetics due to the high acidity of thiol compared to alcohol. This is translated in the higher stability of ruthenium thiolate intermediate with respect to ruthenium alkoxide intermediate. In addition, with the goal of

* Corresponding authors.
E-mail addresses: luismiguel.azofra@ulpgc.es (L.M. Azofra), albert.poater@udg.edu (A. Poater).

https://doi.org/10.1016/j.mcat.2021.111692
Received 11 May 2021; Received in revised form 28 May 2021; Accepted 29 May 2021
Available online 19 June 2021

hydrogenation of thioesters, undesired competitive reaction pathways like the dehydrogenative coupling of alcohol to ester as well as the Tishchenko reaction coupling aldehyde to ester were found out to be not kinetically favored [31,32].

Herein, we investigate the reaction pathway [33] of the catalytic hydrogenation of a series of thioesters by means of sterics through density functional theory (DFT) calculations.

Computational details

DFT calculations were performed using the facilities provided by the Gaussian16 package [34]. For geometry optimization, the GGA-based BP86 functional was used [35,36], including explicit dispersion corrections to the energy through the Grimme D3BJ method [37]. All geometry optimizations were performed without symmetry constraints in the gas phase. The located stationary points were characterized as minima or transition states by analytical frequency calculations. The split-valence basis set Def2-SVP from Ahlrichs and co-workers was used for non-metal atoms [38], while for ruthenium, the small-core, quasi-relativistic Stuttgart/Dresden effective core potential (SDD) was employed [39–41]. For single-point energy refinements, the hybrid GGA-based B3LYP functional was used [42,43] with the Def2-TZVP basis set [44,45]. At this stage, solvent effects were introduced by means of the universal solvation model based on density (SMD) variation of IEFPCM by Truhlar and co-workers [46], using 1,4-dioxane as solvent. Gibbs energies were calculated as the sum of the electronic energies at the B3LYP-D3BJ-SMD(1,4-dioxane)/Def2-TZPV~SDD//BP 86-D3BJ/Def2-SVP~SDD level of theory plus the zero-point energies (ZPE) and thermal corrections calculated at the BP86-D3BJ/Def2-SVP~SDD computational level in vacuum. All free energies refer to standard Gibbs energies in a 1 M standard-state concentration for all species [47–49], *i.e.*, the change of the conventional 1 atm standard state for gas phase calculations to a standard state of 1 M concentration in solution entails corrections of 1.9 and 3.0 kcal/mol at 298.15 and 423.15 K, respectively [50–52].

Results and discussion

The reaction mechanism of the Ru-catalyzed thioester hydrogenation by Milstein and co-workers [26,27] has been unveiled by means of density functional theory (DFT) (See Fig. 2). The process starts with the coordination between the thioester *S*-methyl propanethioate (as model substrate) with the ruthenium-acridine complex ***fac*-Ru**, which presents a vacancy site at the ruthenium center. A significant destabilization of 16.7 kcal/mol is seen leading to a highly sterically impeded complex **1** which allows [53–56], however, the subsequent hydride transfer from ruthenium to the sp^2 carbon of the entering carbonyl group, *i.e.*, the insertion of the thioester into the Ru-H bond of the catalyst [57], overcoming an energy barrier of 12.6 kcal/mol (**TS1**). A relatively unstable hexacoordinated Ru intermediate **2** bearing an agostic interaction is formed, which evolves to the more favored pentacoordinated complex **2a**, breaking the agostic interaction and releasing 7.7 kcal/mol. In this context, the calculation of the sterical hindrance by means of the $\%V_{Bur}$ index defined by Cavallo and co-workers [58–60] decreases from 79.3 to

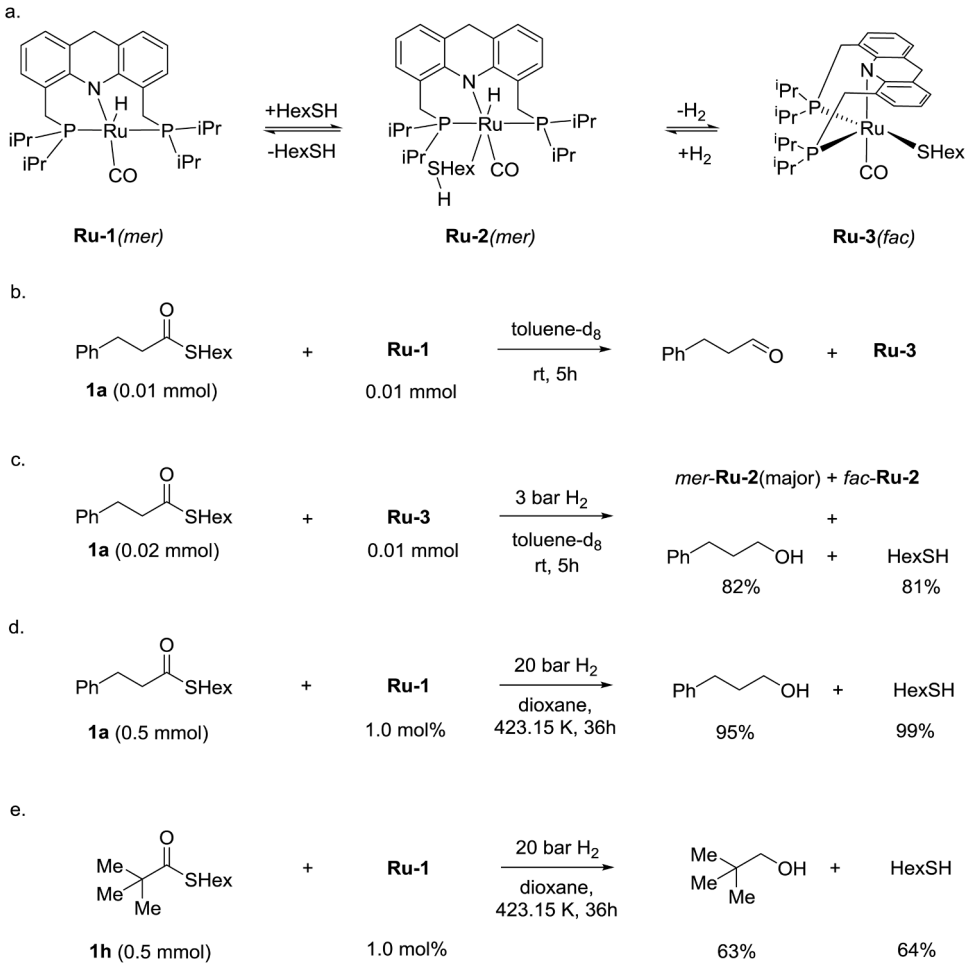

Fig. 1. (a) PNP pincer Ru-based complexes; stoichiometric transformation of thioester (b) to aldehyde by Ru-1 and (c) to alcohol by Ru-3; (d) catalytic transformation of thioester 1a and (e) of thioester 1 h to evaluate the steric effects.

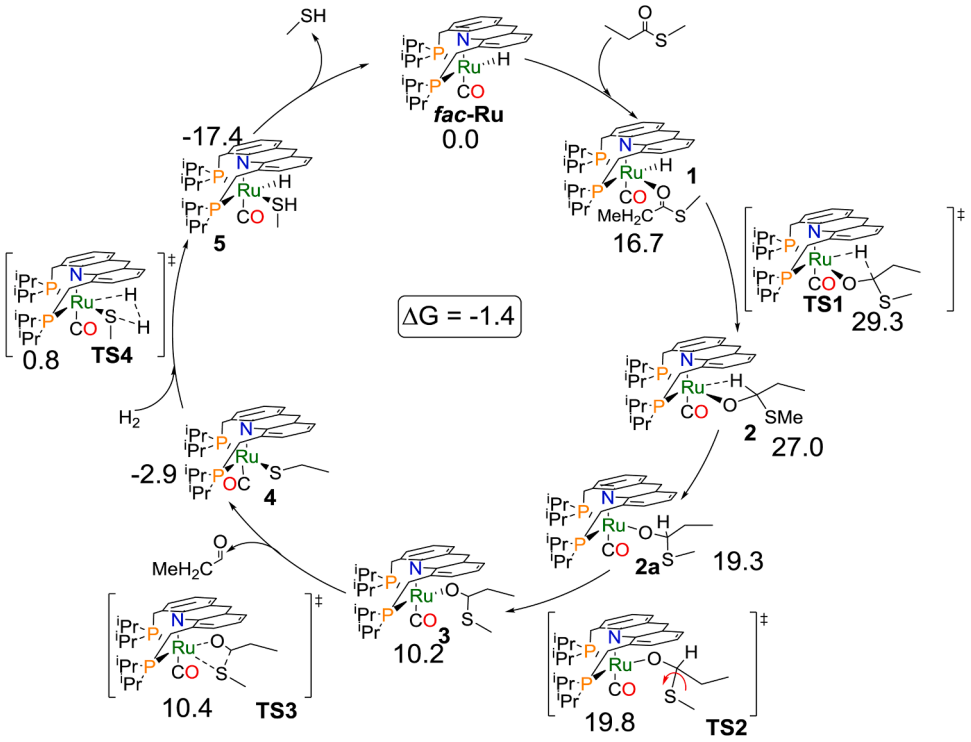

Fig. 2. Reaction mechanism for the Ru-catalyzed thioester hydrogenation using ***fac*-Ru** as catalyst (Relative Gibbs energies in kcal/mol calculated at 298.15 K).

71.4% [61,62]. Next, the nearly barrierless rotational movement around the Ru–O–C–S dihedral angle in **TS2** facilitates the isomerization of complex **2a** into complex **3**, and guides to the subsequent C–S bond cleavage through **TS3** and the release of an aldehyde moiety that leads to the formation of intermediate **4**. The latter thioalkyl transfer *via* **TS3** is also a kinetically irrelevant process with a very low energy barrier of just 0.2 kcal/mol. To close the catalytic cycle, the former ***fac*-Ru** complex is then regenerated through hydrogenation of complex **4** by molecular hydrogen. The heterolytic H–H bond cleavage [63–65] with a kinetic cost of 3.7 kcal/mol *via* **TS4** leads to the formation of the hydride intermediate **5**, prone to release a thiol product in an overall exergonic reaction with a reaction free energy of 1.4 kcal/mol. Although not shown at Fig. 2, complex **5** will be also the active species for the aldehyde hydrogenation into alcohol (previously released) through a so-called **TS5** to regenerate complex **4**, however this should overcome a significant energy barrier of 36.9 kcal/mol.

Overall, the rate-determining step (rds) is imposed by **TS1**. Although a relative barrier of 12.6 kcal/mol is seen with respect complex **1**, according to Shaik and Kozuch [66], the rate determining intermediate as reference is the lowest in energy before the rds, so **TS1** is the single transition state that is responsible for the turnover frequency (TOF) being at 29.3 kcal/mol with respect ***fac*-Ru**.

Since the catalyst performance is actually optimized at 423.15 K, ΔG values at Fig. 2 have been recalculated at this temperature. (See Fig. S1 from the Supporting Information). The value of the rds changes to 33.7 kcal/mol for this case. It should be noted that a comparison of ΔG values at both temperatures explain why at mild conditions the reaction cannot take place: it is necessary to increase the temperature, and although it involves a slight increase in the kinetic cost of the rds, the temperature allows to supply it.

Knowing that the catalytic performance drops for thioesters with higher sterical alkyl groups in alpha to the carbonyl group, substrates **II** (*S*-methyl *t*-butylpropanethioate), **III** [*S*-(*t*-butyl) propanethioate], and **IV** [*S*-(*t*-butyl) *t*-butylpropanethioate] at Scheme 1 have been also considered. Focusing just on **TS1** (rds), the introduction of a *t*-butyl (*t*-Bu) group in the sulfur substituent (**III**) increases the energy barrier by 1.4 kcal/mol, while this is 9.5 kcal/mol if the *t*-Bu substituent is bonded directly to the keto group (**II**). When both sides of substrate **I** are substituted with *t*-Bu groups (**IV**), the barrier increases by 9.8 kcal/mol. Looking at the geometry of **TS1** for each case (Fig. 3), once added the *t*-Bu group(s), it is clear that the sterical hindrance is larger when this bulky substituent is next to the keto group.

Undoubtedly, this high energy barrier is principally caused by the steric hindrance between the substituents of thioesters and the two isopropyl (*i*-Pr) groups on the phosphorous atoms of the PNP pincer ligand. For that reason, $\%V_{Bur}$ between the substituents and the *i*-Pr groups has been calculated for **TS1** with values of 75.7, 82.1, 80.3 and 84.8% for **I-IV** series, respectively. Steric maps in Fig. 4 confirm that the

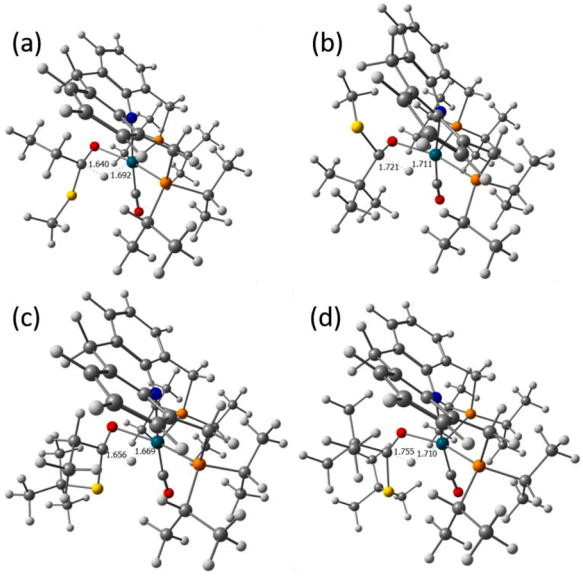

Fig. 3. Rate determining transition state TS1 for (a) I, (b) II, (c) III, and (d) IV substrates. Selected distances are shown in Å.

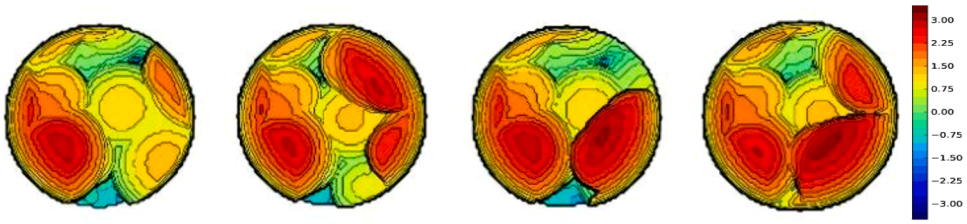

Fig. 4. Topographic steric maps (plane *xy*) with the metal in the *z* axis of the TS1 for I-IV substrates (from left to right), with a radius of 3.5 Å.

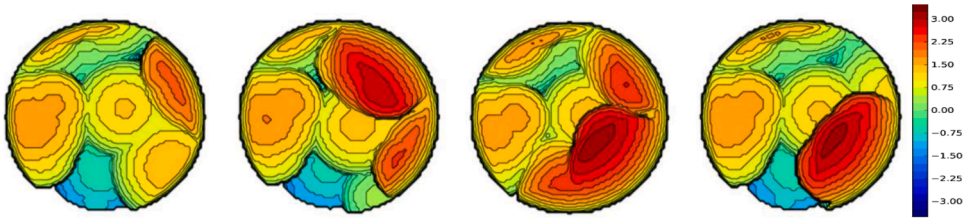

Fig. 5. Topographic steric maps (plane *xy*) with the metal in the *z* axis of the TS1 for I-IV substrates (from left to right), with a radius of 3.5 Å, using *fac*-Ru with methyls on the P atoms of the PNP pincer ligand.

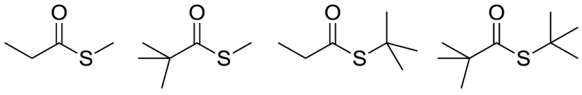

Scheme 1. Scope of substrates.

left groove corresponding to the substituent on the sulfur has a low or even null impact on the active center of **TS1** [67], while on the right groove, the *t*-Bu group has a significant change [68]. It should be noted that the steric maps for substrate **III** would seem that the quadrant on the right and bottom is very obstructed, but this fact is offset by the one above. Quantifying by quadrants, the value of this for substrate **III** is 68.6%, even lower than for **I** (70.5%). For comparison, in substrates **II** and **IV** this increases to 89.7 and 79.6%, respectively.

In the frame of the Conceptual DFT analysis [69], the chemical hardness of intermediate **1** was evaluated, as well as for the **I-IV** substrates separately. In general rules, substrate **IV** is much less reactive than **I**, with **II** and **III** in between, at the electronic level [70,71,72,73]. Hardness values are 69.0, 71.5, 70.3, and 72.2 kcal/mol for complexed **I-IV** substrates at the intermediate **1**. Interestingly, we did not observe any trend for the substrates separately, revealing that what plays a major role is the interaction of the substrates with the catalyst. Even though the *t*-Bu groups have a predominant sterical importance, the electronic nature is also capable of explain the different reactivity between the thioester substrates, following the same trend. We also carried out supporting calculations to analyze the effect of the non-covalent interactions between substrates and ***fac*-Ru** [74]. In this regard, NCIplots calculations by Contreras et al. [75,76] were performed, but no significant differences were appreciated between the four different substrates [77,78].

In an attempt to move to milder conditions, predictive catalytic analysis was employed by simple substitution of the *i*-Pr groups in the phosphines of the PNP pincer ligand by the less sterically demanding hydrogen and methyl groups. Interestingly, the **TS1** rds drop from 29.3 kcal/mol to just 16.4 and 16.2 kcal/mol, respectively, for substrate **I**. In addition, for substrates **II-IV** these values are of just 22.7, 17.6 and 22.5 kcal/mol, respectively, for the catalyst with the phosphines substituted with methyl groups. These free energy barriers are more affordable at room temperature. In addition, steric maps and%V_{Bur} provides a clear explanation about this drop of kinetics demand [79,80]. In detail, the %V_{Bur} for **TS1** decreases from 75.7 to 68.4% for substrate **I**, and with a similar decrease of around 7–8% for the other substrates. The steric maps in Fig. 5 give an even clearer view of the lower steric demand by substituting the *i*-Pr groups groups by methyls of the PNP pincer ligand, specially on the left.

In an attempt to put together the sterics with the electronics, following the scheme of Falivene and Cavallo [81], multilinear regressions were tested with the recognized low amount set of data for such an analysis. Despite the low statistical significance, the agreement was found to be 0.76 for %V_{Bur} and the energy of the LUMO of **TS1**. However, still the main contribution is due to sterics since the agreement with just %V_{Bur} is 0.8888 [82].

Conclusions

By DFT calculations, we have unveiled the reaction mechanism of the catalytic hydrogenation of thioesters to form thiols and alcohols for a series of substrates with different bulky and not bulky substituents, in particular *t*-Bu groups. The results confirmed that the insertion of *t*-Bu groups to the substrate structure was dramatic next to the keto of the thioester chemical group, whereas innocent on the sulfur ligand. We also conducted further predictive calculations modifying the structure of the PNP replacing the *i*-Pr groups on both phosphorous atoms by methyl groups and hydrogen atoms in order to provide a route to milder conditions. Steric maps indicate that the different catalytic performance evaluated here is mainly due to sterics, although Conceptual DFT also confirms the trend since bulky *t*-Bu groups also increase the chemical hardness [83], and, by application of the Principle of Maximum Hardness (PMH) [84], decrease the chemical reactivity.

Authors' contribution'

Michele Tomasini: Calculations, Visualization, Data management, Writing – original draft. **Josep Duran**: Visualization, Data management, Writing – original draft. **Sílvia Simon**: Visualization, Data management, Writing – original draft. **Luis Miguel Azofra**: Conceptualization, Writing – review & editing, Funding acquisition. **Albert Poater:** Conceptualization, Writing – original draft, review & editing, Supervision, Funding acquisition.

Declaration of Competing Interest

The authors declare that they have no known competing financial interests or personal relationships that could have appeared to influence the work reported in this paper.

Acknowledgments

A.P. is a Serra Húnter Fellow and ICREA Academia Prize 2019, and thanks the Spanish MINECO for projects ref. PGC2018-097722-B-I00 and CTQ2017-85341-P. L.M.A. thanks Universidad de Las Palmas de Gran Canaria (ULPGC) for support.

Supplementary materials

Supplementary material associated with this article can be found, in the online version, at doi:10.1016/j.mcat.2021.111692.

Appendix A. Supplementary data

Supplementary material related to this article can be found, in the online version, at doi:https://doi.org/10.1016/j.mcat.2021.XXXXXX.

References

[1] P. Bobbio, Notes- hydrogenolysis of thioesters, J. Org. Chem. 26 (1961) 3023–3024.
[2] T. Fukuyama, S.C. Lin, L. Li, Facile reduction of ethyl thiol esters to aldehydes: application to a total synthesis of (+)-neothramycin A methyl ether, J. Am. Chem. Soc. 112 (1990) 7050–7051.
[3] J.A. Read, C.T. Walsh, The lyngbyatoxin biosynthetic assembly line: chain release by four-electron reduction of a dipeptidyl thioester to the corresponding alcohol, J. Am. Chem. Soc. 129 (2007) 15762–15763.
[4] U.R. Awodi, J.L. Ronan, J. Masschelein, E.L.C. de los Santos, G.L. Challis, Thioester reduction and aldehyde transamination are universal steps in actinobacterial polyketide alkaloid biosynthesis, Chem. Sci. 8 (2017) 411–415.
[5] M.W. Mullowney, R.A. McClure, M.T. Robey, N.L. Kelleher, R.J. Thomson, Natural products from thioester reductase containing biosynthetic pathways, Nat. Prod. Rep. 35 (2018) 847–878.
[6] P.A. Dub, T. Ikariya, Catalytic reductive transformations of carboxylic and carbonic acid derivatives using molecular hydrogen, ACS Catal. 2 (2012) 1718–1741.
[7] S. Werkmeister, K. Junge, M. Beller, Catalytic hydrogenation of carboxylic acid esters, amides, and nitriles with homogeneous catalysts, Org. Process Res. Dev. 18 (2014) 289–302.
[8] J. Pritchard, G.A. Filonenko, R. van Putten, E.J.M. Hensen, E.A. Pidko, Heterogeneous and homogeneous catalysis for the hydrogenation of carboxylic acid derivatives: history, advances and future directions, Chem. Soc. Rev. 44 (2015) 3808–3833.
[9] G.A. Filonenko, R. van Putten, E.J.M. Hensen, E.A. Pidko, Catalytic (de) hydrogenation promoted by non-precious metals-Co, Fe and Mn: recent advances in an emerging field, Chem. Soc. Rev. 47 (2018) 1459–1483.
[10] F. Kallmeier, R. Kempe, Manganese complexes for (De)hydrogenation catalysis: a comparison to cobalt and iron catalysts, Angew. Chem., Int. Ed. 57 (2018) 46–60.
[11] F.M.A. Geilen, B. Engendahl, M. Hölscher, J. Klankermayer, W. Leitner, Selective homogeneous hydrogenation of biogenic carboxylic acids with $[Ru(TriPhos)H]^+$: a mechanistic study, J. Am. Chem. Soc. 133 (2011) 14349–14358.
[12] T.P. Brewster, A.J.M. Miller, D.M. Heinekey, K.I. Goldberg, Hydrogenation of carboxylic acids catalyzed by half-sandwich complexes of iridium and rhodium, J. Am. Chem. Soc. 135 (2013) 16022–16025.
[13] T.J. Korstanje, J. van der Vlugt, C.J. Elsevier, B. de Bruin, Hydrogenation of carboxylic acids with a homogeneous cobalt catalyst, Science 350 (2015) 298–302.
[14] M. Tamura, Y. Nakagawa, K. Tomishige, Recent developments of heterogeneous catalysts for hydrogenation of carboxylic acids to their corresponding alcohols, Asian J. Org. Chem. 9 (2020) 126–143.
[15] U.K. Das, A. Kumar, Y. Ben-David, M.A. Iron, D. Milstein, Manganese catalyzed hydrogenation of carbamates and urea derivatives, J. Am. Chem. Soc. 141 (2019) 12962–12966.
[16] A.M. Smith, R. Whyman, Review of methods for the catalytic hydrogenation of carboxamides, Chem. Rev. 114 (2014) 5477–5510.
[17] E. Balaraman, C. Gunanathan, J. Zhang, L.J.W. Shimon, D. Milstein, Efficient hydrogenation of organic carbonates, carbamates and formates indicates alternative routes to methanol based on CO_2 and CO, Nat. Chem. 3 (2011) 609–614.
[18] J. Yang, A.J. Pell, N. Hedin, A. Lyubartsev, Computational insight into the hydrogenation of CO_2 and carbamic acids to methanol by a ruthenium(II)-based catalyst: the role of amino (NH) ligand group, Mol. Catal. 506 (2021), 111544.
[19] E. Balaraman, B. Gnanaprakasam, L.J.W. Shimon, D. Milstein, Direct hydrogenation of amides to alcohols and amines under mild conditions, J. Am. Chem. Soc. 132 (2010) 16756–16758.
[20] Y. Xie, P. Hu, T. Bendikov, D. Milstein, Heterogeneously catalyzed selective hydrogenation of amides to alcohols and amines, Catal. Sci. Technol. 8 (2018) 2784–2788.
[21] Y.-.Q. Zou, S. Chakraborty, A. Nerush, D. Oren, Y. Diskin-Posner, Y. Ben-David, D. Milstein, Highly Selective, Efficient deoxygenative hydrogenation of amides catalyzed by a manganese pincer complex via metal-ligand cooperation, ACS Catal. 8 (2018) 8014–8019.
[22] T. vom Stein, M. Meuresch, D. Limper, M. Schmitz, M. Hölscher, J. Coetzee, D. J. Cole-Hamilton, J. Klankermayer, W. Leitner, Highly versatile catalytic hydrogenation of carboxylic and carbonic acid derivatives using a Ru-triphos complex: molecular control over selectivity and substrate scope, J. Am. Chem. Soc. 136 (2014) 13217–13225.
[23] L.-.G. Chen, X.-.H. Zhang, Q.-.Y. Liu, Q. Zhang, T.-.J. Wang, C.-.G. Wang, L.-.L. Ma, Research progress on reaction mechanism and catalysts for hydrogenation of carboxylic acids, J. Mol. Catal. 31 (2017) 267–276.
[24] M.L. Clarke, Recent developments in the homogeneous hydrogenation of carboxylic acid esters, Catal. Sci. Technol. 2 (2012) 2418–2423.
[25] T. Zell, Y. Ben-David, D. Milstein, Unprecedented iron-catalyzed ester hydrogenation. Mild, selective, and efficient hydrogenation of trifluoroacetic esters to alcohols catalyzed by an iron pincer complex, Angew. Chem., Int. Ed. 53 (2014) 4685–4689.
[26] J. Luo, M. Rauch, L. Avram, Y. Ben-David, D. Milstein, Catalytic hydrogenation of thioesters, thiocarbamates, and thioamides, J. Am. Chem. Soc. 142 (2020) 21628–21633.
[27] M. Rauch, J. Luo, L. Avram, Y. Ben-David, D. Milstein, Mechanistic investigations of ruthenium catalyzed dehydrogenative thioester synthesis and thioester hydrogenation, ACS Catal. 11 (2021) 2795–2807.
[28] L.M. Azofra, A. Poater, Diastereoselective diazenyl formation: the key for manganese-catalysed alcohol conversion into (E)-alkenes, Dalton Trans. 48 (2019) 14122–14127.
[29] J.A. Luque-Urrutia, M. Solà, D. Milstein, A. Poater, Mechanism of the manganese-pincer-catalyzed acceptorless dehydrogenative coupling of nitriles and alcohols, J. Am. Chem. Soc. 141 (2019) 2398–2403.
[30] J. Masdemont, J.A. Luque-Urrutia, M. Gimferrer, D. Milstein, A. Poater, Mechanism of coupling of alcohols and amines to generate aldimines and H_2 by a pincer manganese catalyst, ACS Catal. 9 (2019) 1662–1669.
[31] J. Zhang, G. Leitus, Y. Ben-David, D. Milstein, Efficient homogeneous catalytic hydrogenation of esters to alcohols, Angew. Chem., Int. Ed. 45 (2006) 1113–1115.
[32] M. Henrion, T. Roisnel, J.-.L. Couturier, J.-.L. Dubois, J.-.B. Sortais, C. Darcel, J.-.F. Carpentier, Ruthenium complexes bearing amino-bis(phosphinite) or amino-bis (aminophosphine) ligands: application in catalytic ester hydrogenation, Mol. Catal. 432 (2017) 15–22.
[33] M. Rosales, K. Molina, F. Arrieta, D. Fernández, P.J. Baricelli, Kinetics and mechanisms of homogeneous catalytic reactions. Part 16. Regioselective hydrogenation of quinoline catalyzed by dichlorotris(triphenylphosphine) ruthenium(II), Mol. Catal. 490 (2020), 110970.
[34] M.J. Frisch, G.W. Trucks, H.B. Schlegel, G.E. Scuseria, M.A. Robb, J.R. Cheeseman, G. Scalmani, V. Barone, G.A. Petersson, H. Nakatsuji, X. Li, M. Caricato, A. V. Marenich, J. Bloino, B.G. Janesko, R. Gomperts, B. Mennucci, H.P. Hratchian, J. V. Ortiz, A.F. Izmaylov, J.L. Sonnenberg, D. Williams-Young, F. Ding, F. Lipparini, F. Egidi, J. Goings, B. Peng, A. Petrone, T. Henderson, D. Ranasinghe, V. G. Zakrzewski, J. Gao, N. Rega, G. Zheng, W. Liang, M. Hada, M. Ehara, K. Toyota, R. Fukuda, J. Hasegawa, M. Ishida, T. Nakajima, Y. Honda, O. Kitao, H. Nakai, T. Vreven, K. Throssell, J.A. Montgomery Jr., J.E. Peralta, F. Ogliaro, M. J. Bearpark, J.J. Heyd, E.N. Brothers, K.N. Kudin, V.N. Staroverov, T.A. Keith, R. Kobayashi, J. Normand, K. Raghavachari, A.P. Rendell, J.C. Burant, S.S. Iyengar, J. Tomasi, M. Cossi, J.M. Millam, M. Klene, C. Adamo, R. Cammi, J.W. Ochterski, R.L. Martin, K. Morokuma, O. Farkas, J.B. Foresman, D.J. Fox, Gaussian 16, Revision C.01, Gaussian, Inc., Wallingford CT, 2016.
[35] A.D. Becke, Density-functional exchange-energy approximation with correct asymptotic behavior, Phys. Rev. A 38 (1988) 3098–3100.
[36] J.P. Perdew, Density-functional approximation for the correlation energy of the inhomogeneous electron gas, Phys. Rev. B 33 (1986) 8822–8824.
[37] S. Grimme, J. Antony, S. Ehrlich, H. Krieg, A consistent and accurate ab initio parametrization of density functional dispersion correction (DFT-D) for the 94 elements H-Pu, J. Chem. Phys. 132 (2010), 154104.
[38] A. Schäfer, H. Horn, R. Ahlrichs, Fully optimized contracted Gaussian basis sets for atoms Li to Kr, J. Chem. Phys. 97 (1992) 2571–2577.
[39] U. Häussermann, M. Dolg, H. Stoll, H. Preuss, P. Schwerdtfeger, R.M. Pitzer, Accuracy of energy-adjusted quasirelativistic ab initio pseudopotentials, Mol. Phys. 78 (1993) 1211–1224.
[40] T. Leininger, A. Nicklass, H. Stoll, M. Dolg, P. Schwerdtfeger, The accuracy of the pseudopotential approximation. II. A comparison of various core sizes for indium pseudopotentials in calculations for spectroscopic constants of InH, InF, and InCl, J. Chem. Phys. 105 (1996) 1052–1059.
[41] W. Küchle, M. Dolg, H. Stoll, H. Preuss, Energy-adjusted pseudopotentials for the actinides. Parameter sets and test calculations for thorium and thorium monoxide, J. Chem. Phys. 100 (1994) 7535–7542.
[42] A.D. Becke, Density-functional thermochemistry. III. The role of exact exchange, J. Chem. Phys. 98 (1993) 5648–5652.
[43] C. Lee, W. Yang, R.G. Parr, Development of the Colle-Salvetti correlation-energy formula into a functional of the electron density, Phys. Rev. B 37 (1988) 785–789.

[44] F. Weigend, R. Ahlrichs, Balanced basis sets of split valence, triple zeta valence and quadruple zeta valence quality for H to Rn: design and assessment of accuracy, Phys. Chem. Chem. Phys. 7 (2005) 3297–3305.
[45] F. Weigend, Accurate Coulomb-fitting basis sets for H to Rn, Phys. Chem. Chem. Phys. 8 (2006) 1057–1065.
[46] A.V. Marenich, C.J. Cramer, D.G. Truhlar, Universal solvation model based on solute electron density and on a continuum model of the solvent defined by the bulk dielectric constant and atomic surface tensions, J. Phys. Chem. B 113 (2009) 6378–6396.
[47] C.P. Kelly, C.J. Cramer, D.G. Truhlar, SM6: a density functional theory continuum solvation model for calculating aqueous solvation free energies of neutrals, ions, and solute-water clusters, J. Chem. Theory Comput. 1 (2005) 1133–1152.
[48] C.P. Kelly, C.J. Cramer, D.G. Truhlar, Aqueous solvation free energies of ions and ion-water clusters based on an accurate value for the absolute aqueous solvation free energy of the proton, J. Phys. Chem. B 110 (2006) 16066–16081.
[49] J.A. Luque-Urrutia, T. Pèlachs, M. Solà, A. Poater, Double-carrousel mechanism for Mn-catalyzed dehydrogenative amide synthesis from alcohols and amines, ACS Catal. 11 (2021) 6155–6161.
[50] V.S. Bryantsev, M.S. Diallo, W.A. Goddard III, Calculation of solvation free energies of charged solutes using mixed cluster/continuum models, J. Phys. Chem. B 112 (2008) 9709–9719.
[51] L. Falivene, V. Barone, G. Talarico, Unraveling the role of entropy in tuning unimolecular vs. bimolecular reaction rates: the case of olefin polymerization catalyzed by transition metals, Mol. Catal. 452 (2018) 138–144.
[52] W. Natongchai, J.A. Luque-Urrutia, Ch. Phyngpanyia, M. Solà, V. D'Elia, A. Poater, H. Zipse, Cycloaddition of CO_2 to epoxides by highly nucleophilic 4-aminopyridines: establishing a relationship between carbon basicity and catalytic performance by experimental and DFT investigations, Org. Chem. Front. 8 (2021) 249–253.
[53] R. Mariz, A. Poater, M. Gatti, E. Drinkel, J.J. Bürgi, X. Luan, S. Blumentritt, A. Linden, L. Cavallo, R. Dorta, C2-symmetric chiral disulfoxide ligands in rhodium-catalyzed 1,4-addition: from ligand synthesis to the enantioselection pathway, Chem. Eur. J. 16 (2010) 14335–14347.
[54] M.O. Albalawi, L. Falivene, A. Jedidi, O.I. Osman, S.A. Elroby, L. Cavallo, Influence of the anionic ligands on properties and reactivity of Hoveyda-Grubbs catalysts, Mol. Catal. 509 (2021), 111612.
[55] S. Manzini, A. Poater, D.J. Nelson, L. Cavallo, S.P. Nolan, How phenyl makes a difference: mechanistic insights into the ruthenium(II)-catalysed isomerisation of allylic alcohols, Chem. Sci. 5 (2014) 180–188.
[56] A. Collado, J. Balogh, S. Meiries, A.M.Z. Slawin, L. Falivene, L. Cavallo, S.P. Nolan, Steric and electronic parameters of a bulky yet flexible N-heterocyclic carbene: 1,3-bis(2,6-bis(1-ethylpropyl)phenyl)imidazol-2-ylidene (IPent), Organometallics 33 (2013) 3249–3252.
[57] Y. Ben-David, M. Gozin, M. Portnoy, D. Milstein, Reductive dechlorination of aryl chlorides catalyzed by palladium complexes containing basic, chelating phosphines, J. Mol Catal. 73 (1986) 173–180.
[58] A. Poater, B. Cosenza, A. Correa, S. Giudice, F. Ragone, V. Scarano, L. Cavallo, SambVca: a web application for the calculation of the buried volume of N-heterocyclic carbene ligands, Eur. J. Inorg. Chem. 2009 (2009) 1759–1766.
[59] H. Jacobsen, A. Correa, A. Poater, C. Costabile, L. Cavallo, Understanding the M(NHC) (NHC = N-heterocyclic carbene) bond, Coord. Chem. Rev. 253 (2009) 687–703.
[60] L. Falivene, R. Credendino, A. Poater, A. Petta, L. Serra, R. Oliva, V. Scarano, L. Cavallo, SambVca 2. A web tool for analyzing catalytic pockets with topographic steric maps, Organometallics 35 (2016) 2286–2293.
[61] A. Hanifpour, N. Bahri-Laleh, M. Nekoomanesh-Haghighi, A. Poater, Group IV diamine bis(phenolate) catalysts for 1-decene oligomerization, Mol. Catal. 493 (2020), 111047.
[62] L. Falivene, L. Cavallo, G. Talarico, Buried volume analysis for propene polymerization catalysis promoted by group 4 metals: a tool for molecular mass prediction, ACS Catal. 5 (2015) 6815–6822.
[63] U. Gellrich, J.R. Khusnutdinova, G.M. Leitus, D. Milstein, Mechanistic investigations of the catalytic formation of lactams from amines and water with liberation of H_2, J. Am. Chem. Soc. 137 (2015) 4851–4859.
[64] X. Ye, P.N. Plessow, M.K. Brinks, M. Schelwies, T. Schaub, F. Rominger, R. Paciello, M. Limbach, P. Hofmann, Alcohol amination with ammonia catalyzed by an acridine-based ruthenium pincer complex: a mechanistic study, J. Am. Chem. Soc. 136 (2014) 5923–5929.
[65] J. Luo, M. Rauch, L. Avram, Y. Diskin-Posner, G. Shmul, Y. Ben-David, D. Milstein, Formation of thioesters by dehydrogenative coupling of thiols and alcohols with H_2 evolution, Nat. Catal. 3 (2020) 887–892.
[66] S. Kozuch, S. Shaik, How to conceptualize catalytic cycles? The energetic span model, Acc. Chem. Res. 44 (2011) 101–110.
[67] L. Falivene, Z. Cao, A. Petta, L. Serra, A. Poater, R. Oliva, V. Scarano, L. Cavallo, Towards the online computer-aided design of catalytic pockets, Nat. Chem. 11 (2019) 872–879.
[68] J.A. Luque-Urrutia, A. Poater, The fundamental non innocent role of water for the hydrogenation of nitrous oxide by PNP pincer Ru-based catalysts, Inorg. Chem. 56 (2017) 14383–14387.
[69] P. Geerlings, F. De Proft, W. Langenaeker, Conceptual density functional theory, Chem. Rev. 103 (2003) 1793–1874.
[70] A. Poater, A. Gallegos Saliner, M. Solà, L. Cavallo, A.P. Worth, Computational methods to predict the reactivity of nanoparticles through structure-property relationships, Expert Opin. Drug Deliv. 7 (2010) 295–305.
[71] M. Costas, X. Ribas, A. Poater, J.M. López-Valbuena, R. Xifra, A. Company, M. Duran, M. Solà, A. Llobet, M. Corbella, M.A. Usón, J. Mahía, X. Solans, X. Shan, J. Benet-Buchholz, Copper(II) hexaaza macrocyclic binuclear complexes obtained from the reaction of their copper(I) derivates and molecular dioxygen, Inorg. Chem. 45 (2006) 3569–3581.
[72] A.R. Shaikh, M. Ashraf, T. AlMayef, M. Chawla, A. Poater, L. Cavallo, Amino acid ionic liquids as potential candidates for CO_2 capture: combined density functional theory and molecular dynamics simulations, Chem. Phys. Lett. 745 (2020), 137239.
[73] M. Fallah, N. Bahri-Laleh, K. Didehban, A. Poater, Interaction of common cocatalysts in Ziegler-Natta catalyzed olefin polymerization, Appl. Organomet. Chem. (2020) e5333.
[74] L. Falivene, L. Cavallo, G. Talarico, The role of noncovalent interactions in olefin polymerization catalysis: a further look to the fluorinated ligand effect, Mol. Catal. 494 (2020), 111118.
[75] E.R. Johnson, S. Keinan, P. Mori-Sánchez, J. Contreras-García, A.J. Cohen, W. Yang, Revealing noncovalent interactions, J. Am. Chem. Soc. 132 (2010) 6498–6506.
[76] J. Contreras-García, E.R. Johnson, S. Keinan, R. Chaudret, J.-.P. Piquemal, D. N. Beratan, W. Yang, NCIPLOT: a program for plotting noncovalent interaction regions, J. Chem. Theory Comput. 7 (2011) 625–632.
[77] S. Dehghani, S. Sadjadi, N. Bahri-Laleh, M. Nekoomanesh-Haghighi, A. Poater, Study of the effect of the ligand structure on the catalytic activity of Pd@ ligand decorated halloysite: combination of experimental and computational studies, Appl. Organomet. Chem. 33 (2019) e4891.
[78] M. Tabrizi, S. Sadjadi, G. Pareras, M. Nekoomanesh-Haghighi, N. Bahri-Laleh, A. Poater, Efficient hydro-finishing of polyalfaolefin based lubricants under mild reaction condition using Pd on ligands decorated halloysite, J. Colloid Interface Sci. 581 (2021) 939–953.
[79] M. Rouen, P. Queval, E. Borré, L. Falivene, A. Poater, M. Berthod, F. Hugues, L. Cavallo, O. Baslé, H. Olivier-Bourbigou, M. Mauduit, Selective metathesis of α-Olefins from bio-sourced Fischer-Tropsch feeds, ACS Catal. 6 (2016) 7970–7976.
[80] A. Poater, L. Falivene, C.A. Urbina-Blanco, S. Manzini, S.P. Nolan, L. Cavallo, How does the addition of steric hindrance to a typical N-heterocyclic carbene ligand affect catalytic activity in olefin metathesis? Dalton Trans. 42 (2013) 7433–7439.
[81] L. Falivene, L. Cavallo, Theoretical NMR spectroscopy of N-heterocyclic carbenes and their metal complexes, Coord. Chem. Rev. 344 (2017) 101–114.
[82] S. Manzini, C.A. Urbina-Blanco, D.J. Nelson, A. Poater, T. Lebl, S. Meiries, A.M. Z. Slawin, L. Falivene, L. Cavallo, S.P. Nolan, Evaluation of an olefin metathesis pre-catalyst with a bulky and electron-rich N-heterocyclic carbene, J. Organomet. Chem. 780 (2015) 43–48.
[83] L.M. Azofra, J. Elguero, I. Alkorta, A conceptual DFT Study of phosphonate dimers: dianions supported by H-bonds, J. Phys. Chem. A 124 (2020) 2207–2214.
[84] R.G. Parr, P.K. Chattaraj, Principle of maximum hardness, J. Am. Chem. Soc. 113 (1991) 1854–1855.